Anisotropy of Magnetoacoustic Attenuation and Deformation Potential in Bismuth

K. WALTHER
Philips Zentrallaboratorium GmbH, Hamburg, Germany
(Received 8 May 1968)

The tensor components C_{ik} of the deformation potential for electrons and holes in bismuth were evaluated from the anisotropy of quantum oscillations in the magnetoacoustic attenuation, measured at a frequency $f=60$ MHz and a temperature $T=1.6$°K. The sign of the deformation potential cannot be determined by this method. The present results confirm the piezogalvanomagnetic measurements of Jain and Jaggi and, in addition to these, yield the shear components. The results are (a) deformation potential for principal electron ellipsoid: $C_{11}/C_{22}=-0.37$, $C_{33}/C_{22}=-0.29$, $C_{23}/C_{22}=+0.25$, and $C_{22}=\pm 5.9$ eV, and (b) deformation potential for hole ellipsoid: $C_{33}/C_{22}=-1.03$ and $C_{33}=\pm 1.2$ eV.

I. INTRODUCTION

In a typical semimetal like bismuth with equal electron and hole concentrations ranging around 3×10^{17} cm^{-3} the interaction between charge carriers and ultrasonic waves with frequencies above 10 MHz is dominated by the deformation potential. The contribution of the self-consistent field is negligible. At sufficiently low temperatures and high magnetic fields the motion of the charge carriers in the plane perpendicular to a magnetic field B is quantized. Sharp spikes ("giant" quantum oscillations) occur in the ultrasonic attenuation as a function of magnetic field (periodic in $1/B$), whenever a Landau level, accompanied by a singularity in the density of states, crosses the Fermi energy. These giant quantum oscillations in the magnetoacoustic attenuation of bismuth at low temperatures were observed by several authors both under attenuating[1–6] and amplifying conditions.[7,8] The theory of acoustic quantum oscillations, including the anisotropy of the Fermi surface and the effects due to impurity scattering, was developed extensively.[9–15] Since the attenuation peaks are very narrow at low temperatures, the oscillation patterns due to the three electron bands and the hole band in bismuth can be separated clearly by means of the magnetic field. In previous experiments,[1–6] the main emphasis was placed on determining the periods $\Delta(1/B)$, spin splitting, and line shape of the giant quantum oscillations.

Inoue and Tsuji[16] investigated the anisotropy of the peak absorption of giant quantum oscillations in bismuth as a function of magnetic field direction by analyzing experimental data for longitudinal waves published by Mase *et al.*[5] The authors[16] estimated the ratio of two deformation-potential tensor components, using the experimental result that the rotated electron ellipsoids do not couple with the quasilongitudinal wave along the bisectrix direction. This information was combined with the parameters describing the dependence of energy overlap between conduction and valence bands on mechanical strain, as determined from piezogalvanomagnetic measurements by Jain and Jaggi.[17] In this way, Inoue and Tsuji[16] could determine several elements of the deformation-potential tensors of electrons and holes in bismuth. However, no information on the shear components of the deformation potential was available, since only longitudinal waves were investigated and since in the piezogalvanomagnetic experiments static shear deformations could not be applied because of easy twinning of the bismuth single crystals.

In the present paper, all components of the deformation-potential tensors of electrons and holes in bismuth are determined by measuring the anisotropy of the peak attenuation of giant quantum oscillations of both longitudinal and shear waves with different directions of propagation and polarization. The experiments were carried out at a frequency of 60 MHz and a temperature $T=1.6$°K. The different components of the deformation-potential tensors can be measured in a direct way and with considerable redundancy. The present ultrasonic measurements confirm the result of the piezogalvanomagnetic investigations[17] and, in addition, yield the shear components of the deformation potential.

[1] D. H. Reneker, Phys. Rev. **115**, 303 (1959).
[2] A. P. Korolyuk, Fiz. Tverd. Tela **5**, 3323 (1963) [English transl.: Soviet Phys.—Solid State **5**, 2433 (1964)].
[3] A. M. Toxen and S. Tansal, Phys. Rev. **137**, A211 (1965).
[4] A. P. Korolyuk, Zh. Eksperim. i Teor. Fiz. **51**, 697 (1966) [English transl.: Soviet Phys.—JETP **24**, 461 (1967)].
[5] S. Mase, Y. Fujimori, and H. Mori, J. Phys. Soc. Japan **21**, 1744 (1966).
[6] Y. Sawada, E. Burstein, and L. Testardi, J. Phys. Soc. Japan Suppl. **21**, 760 (1966).
[7] K. Walther, Phys. Rev. Letters **16**, 642 (1966).
[8] K. Walther, Z. Naturforsch. **21a**, 1443 (1966).
[9] V. L. Gurevich, V. G. Skobov, and Y. A. Firsov, Zh. Eksperim. i Teor. Fiz. **40**, 786 (1961) [English transl.: Soviet Phys.—JETP **13**, 552 (1961)].
[10] V. G. Skobov, Zh. Eksperim. i Teor. Fiz. **40**, 1446 (1961) [English transl.: Soviet Phys.—JETP **13**, 1014 (1961)].
[11] J. J. Quinn and S. Rodriguez, Phys. Rev. **128**, 2487 (1962); **128**, 2494 (1962).
[12] S. V. Gantsevich and V. L. Gurevich, Zh. Eksperim. i Teor. Fiz. **45**, 587 (1963) [English transl.: Soviet Phys.—JETP **18**, 403 (1964)].
[13] J. J. Quinn, Phys. Rev. **135**, A181 (1964).
[14] J. J. Quinn, Phys. Rev. **137**, A889 (1965).
[15] S. H. Liu and A. M. Toxen, Phys. Rev. **138**, A487 (1965).
[16] S. Inoue and M. Tsuji, J. Phys. Soc. Japan **22**, 1191 (1967).
[17] A. L. Jain and R. Jaggi, Phys. Rev. **135**, A708 (1964).

II. THEORY

A. Deformation Potential of Electrons and Holes in Bismuth

The change of energy of a charge carrier under the influence of a mechanical deformation of the crystal is given by[18]

$$\delta\phi=\mathbf{C}:\boldsymbol{\varepsilon}=\sum_{i,k}C_{ik}\epsilon_{ik}, \tag{1}$$

where $\mathbf{C}=C_{ik}$ is the tensor of the deformation potential and $\boldsymbol{\varepsilon}=\epsilon_{ik}$ is the tensor of the mechanical strain. For a plane sound wave with a wave vector $\mathbf{q}$ ($\hat{q}=\mathbf{q}/q$ being the unit vector in the direction of the wave normal) and a polarization in the direction of the unit vector $\hat{e}$, the mechanical displacement $\mathbf{u}$ is proportional to

$$\hat{e}\exp[i(\omega t-\mathbf{q}\cdot\mathbf{r})],$$

where ω is the angular frequency. The strain-tensor components for the ultrasonic wave are given by

$$\epsilon_{ik}=\tfrac{1}{2}(\partial u_i/\partial x_k+\partial u_k/\partial x_i)\sim\tfrac{1}{2}(e_iq_k+e_kq_i), \tag{2}$$

e_i and q_k are the components of the unit vectors $\hat{e}$ and $\hat{q}$. Since $C_{ik}=C_{ki}$, Eq. (1) can be written

$$\delta\phi\sim\hat{e}\cdot\mathbf{C}\cdot\hat{q}=\sum_{i,k}C_{ik}e_iq_k. \tag{3}$$

The deformation-potential tensor $\mathbf{C}$ transforms in the same way as the tensor $\boldsymbol{\alpha}$ of the reciprocal effective mass under the symmetry operations of the crystal.

The Fermi surface of electrons and holes in bismuth will be considered in the ellipsoidal-parabolic approximation (EP model). All physical quantities will be described in terms of the following crystallographic coordinate system: x is the binary axis, y is the bisectrix, and z is the trigonal axis. The Fermi surface of electrons consists of three ellipsoids, located at the centers of the pseudohexagonal faces (L points) of the Brillouin zone.[19] The reciprocal effective mass (in units of m_0^{-1}, where m_0 is the free-electron mass) of the three electron bands is described by the tensors $\boldsymbol{\alpha}^{(l)}$, where $l=1$ refers to the principal ellipsoid in the xyz system, and the ellipsoids with $l=2$ and 3 are rotated by $\pm120°$ around the z axis. One principal axis of the ellipsoid with $l=1$ is parallel to the x axis, and the other two principal axes are tilted by an angle $\vartheta_t\approx6°$ against the yz system. The components of the $\boldsymbol{\alpha}$ tensor for the principal electron ellipsoid are given by ($\alpha_{ik}=\alpha_{ki}$):

$$\begin{aligned}&\alpha_{11}{}^{(1)}=\alpha_1, && \alpha_{22}{}^{(1)}=\alpha_2, && \alpha_{33}{}^{(1)}=\alpha_3,\\ &\alpha_{12}{}^{(1)}=\alpha_{13}{}^{(1)}=0, && \alpha_{23}{}^{(1)}=\alpha_4,\end{aligned} \tag{4}$$

where $\tan2\vartheta_t=2\alpha_4/(\alpha_3-\alpha_2)$. The Fermi surface of holes consists of one ellipsoid of revolution around the trigonal axis, located at the center of the hexagonal face (T point) of the Brillouin zone.[19] The reciprocal effective mass for holes is described by the tensor $\boldsymbol{\alpha}^{(l)}$ with $l=4$ with the components

$$\begin{aligned}&\alpha_{11}{}^{(4)}=\alpha_{22}{}^{(4)}=\beta_1, && \alpha_{33}{}^{(4)}=\beta_2,\\ &\alpha_{12}{}^{(4)}=\alpha_{13}{}^{(4)}=\alpha_{23}{}^{(4)}=0.\end{aligned} \tag{5}$$

The deformation-potential tensors $\mathbf{C}^{(l)}$ for these energy bands can be written in the following general form:

Principal electron ellipsoid ($l=1$):

$$\begin{aligned}&C_{11}{}^{(1)}=a_1, && C_{22}{}^{(1)}=a_2, && C_{33}{}^{(1)}=a_3,\\ &C_{12}{}^{(1)}=C_{13}{}^{(1)}=0, && C_{23}{}^{(1)}=a_4;\end{aligned} \tag{6}$$

rotated electron ellipsoids ($l=2, 3$):

$$\begin{aligned}&C_{11}{}^{(2,3)}=\tfrac{1}{4}(a_1+3a_2), && C_{22}{}^{(2,3)}=\tfrac{1}{4}(3a_1+a_2), && C_{33}{}^{(2,3)}=a_3,\\ &C_{12}{}^{(2,3)}=\pm\tfrac{1}{4}\sqrt{3}(a_1-a_2), && C_{13}{}^{(2,3)}=\pm\tfrac{1}{2}\sqrt{3}a_4, && C_{23}{}^{(2,3)}=-\tfrac{1}{2}a_4;\end{aligned} \tag{7}$$

hole ellipsoid ($l=4$):

$$\begin{aligned}&C_{11}{}^{(4)}=C_{22}{}^{(4)}=b_1, && C_{33}{}^{(4)}=b_2,\\ &C_{12}{}^{(4)}=C_{13}{}^{(4)}=C_{23}{}^{(4)}=0.\end{aligned} \tag{8}$$

In order to find the deformation potential [see Eq. (3)] for various ultrasonic modes in bismuth, the polarization vectors $\hat{e}$ for a given direction of the wave vector $\hat{q}$ were calculated from the elastic constants[20,21] using elasticity theory.[22] The pertinent quantities for sound propagation along the directions $\hat{x}$, $\hat{y}$, $\hat{z}$, and $\frac{1}{2}\sqrt{2}(\hat{y}+\hat{z})$ are summarized in Table I. The values of the sound velocity v_s, listed in Table I, refer to the temperature $T=4.2°$K. Some velocities were determined directly at 4.2°K by Reneker,[1] and other values of v_s were extrapolated from room-temperature data.[20] Table I shows that measurements with $\hat{q}\|\hat{x}$ and $\hat{y}$ are suitable for determining combinations between the deformation-potential components a_1, a_2, and a_4 for electrons and b_1 for holes. With ultrasonic propagation along the directions $\hat{z}$ and $\frac{1}{2}\sqrt{2}(\hat{y}+\hat{z})$ the constants a_3 for electrons and b_2 for holes can be obtained.

B. Quantum Oscillations of the Magnetoacoustic Attenuation in Bismuth

For a single ellipsoidal-parabolic energy band the energy levels in the presence of a quantizing magnetic field B are given by

$$E_{n,s}(k_B)=(n+\tfrac{1}{2})\hbar\omega_c+\hbar^2k_B{}^2/2m_0m_B+sg\mu_BB \qquad (n=0, 1, 2, \cdots, s=\pm\tfrac{1}{2}). \tag{9}$$

The first term describes the quantization of the cyclotron motion in the plane perpendicular to $\mathbf{B}$ with orbital

[18] R. W. Keyes, J. Electron. **2**, 279 (1956).
[19] S. H. Koenig, A. A. Lopez, D. B. Smith, and J. L. Yarnell, Phys. Rev. Letters **20**, 48 (1968).
[20] Y. Eckstein, A. W. Lawson, and D. H. Reneker, J. Appl. Phys. **31**, 1534 (1960).
[21] S. Epstein and A. P. de Bretteville, Jr., Phys. Rev. **138**, A771 (1965).
[22] W. P. Mason, *Physical Acoustics and the Properties of Solids* (D. Van Nostrand Co., Inc., Princeton, N. J., 1958), p. 368.

TABLE I. Deformation potentials for various ultrasonic modes in bismuth.

Wave-vector direction	Mode	Sound velocity v_s (10^5 cm/sec)	Polarization vector $\hat{e}$	Band index l	Deformation potential $\sum_{i,k} C_{ik}e_i q_k$
	L	2.62	$\begin{bmatrix}1\\0\\0\end{bmatrix}$	1	a_1
				2, 3	$\frac{1}{4}(a_1+3a_2)$
				4	b_1
$\begin{bmatrix}1\\0\\0\end{bmatrix}$	S_1	1.64	$\begin{bmatrix}0\\0.8632\\0.5048\end{bmatrix}$	1	0
				2, 3	$\pm\frac{1}{2}\sqrt{3}[0.4316(a_1-a_2)+0.5048a_4]$
				4	0
	S_2	0.892	$\begin{bmatrix}0\\0.5048\\-0.8632\end{bmatrix}$	1	0
				2, 3	$\pm\frac{1}{2}\sqrt{3}[0.2524(a_1-a_2)-0.8632a_4]$
				4	0
	L	2.70	$\begin{bmatrix}0\\-0.9909\\0.1349\end{bmatrix}$	1	$[-0.9909a_2+0.1349a_4]$
				2, 3	$\frac{1}{4}[-0.9909(3a_1+a_2)-0.2697a_4]$
				4	$-0.9909b_1$
$\begin{bmatrix}0\\1\\0\end{bmatrix}$	S_1	1.477	$\begin{bmatrix}1\\0\\0\end{bmatrix}$	1	0
				2, 3	$\pm\frac{1}{4}\sqrt{3}(a_1-a_2)$
				4	0
	S_2	1.073	$\begin{bmatrix}0\\0.1349\\0.9909\end{bmatrix}$	1	$[0.1349a_2+0.9909a_4]$
				2, 3	$\frac{1}{4}[0.1349(3a_1+a_2)-1.9817a_4]$
				4	$0.1349b_1$
	L	2.02	$\begin{bmatrix}0\\0\\1\end{bmatrix}$	1–3	a_3
				4	b_2
$\begin{bmatrix}0\\0\\1\end{bmatrix}$	S	1.13	$\begin{bmatrix}\cos\vartheta\\\sin\vartheta\\0\end{bmatrix}$	1	a_4
				2, 3	$\frac{1}{2}(\pm\sqrt{3}\cos\vartheta-\sin\vartheta)a_4$
				4	0
	L	2.145	$\begin{bmatrix}0\\0.7696\\0.6385\end{bmatrix}$	1	$\frac{1}{2}\sqrt{2}(0.7696a_2+0.6385a_3+1.4081a_4)$
				2, 3	$\frac{1}{8}\sqrt{2}[0.7696(3a_1+a_2)+2.5540a_3-2.8162a_4]$
				4	$\frac{1}{2}\sqrt{2}(0.7696b_1+0.6385b_2)$
$\begin{bmatrix}0\\\frac{1}{2}\sqrt{2}\\\frac{1}{2}\sqrt{2}\end{bmatrix}$	S_1	1.60	$\begin{bmatrix}1\\0\\0\end{bmatrix}$	1	0
				2, 3	$\pm\frac{1}{4}(\sqrt{\frac{3}{2}})(a_1-a_2+2a_4)$
				4	0
	S_2	1.208	$\begin{bmatrix}0\\0.6385\\-0.7696\end{bmatrix}$	1	$\frac{1}{2}\sqrt{2}(0.6385a_2-0.7696a_3-0.1311a_4)$
				2, 3	$\frac{1}{8}\sqrt{2}[0.6385(3a_1+a_2)-3.0785a_3+0.2623a_4]$
				4	$\frac{1}{2}\sqrt{2}(0.6385b_1-0.7696b_2)$

quantum number n, where

$$\omega_c=(e/m_0m_c)B \tag{10a}$$

is the cyclotron frequency,

$$m_c=[(\det\mathbf{m})/(\hat{B}\cdot\mathbf{m}\cdot\hat{B})]^{1/2} \tag{10b}$$

is the cyclotron mass, $\mathbf{m}$ is the tensor of effective mass in units of m_0, and $\hat{B}$ is the unit vector in the direction of $\mathbf{B}$. The second term in Eq. (9) refers to the translational motion of the charge carriers in the direction of the magnetic field, where k_B and $m_B=\hat{B}\cdot\mathbf{m}\cdot\hat{B}$ are the wave number and effective mass parallel to $\hat{B}$, respectively. The third term in Eq. (9) gives the spin splitting of the Landau levels due to an anisotropic g factor, where μ_B is the Bohr magneton and $s=\pm\frac{1}{2}$ is the spin quantum number. The g factor can be expressed in terms of a spin mass m_s, which is calculated from a tensor $\mathbf{m}_s$:

$$g=2/m_s,\quad m_s=[(\det\mathbf{m}_s)/(\hat{B}\cdot\mathbf{m}_s\cdot\hat{B})]^{1/2}. \tag{11}$$

Equation (9) can be rewritten as

$$E_{n,s}(k_B)=(n+\tfrac{1}{2}+s\Delta)\hbar\omega_c+\hbar^2k_B^2/2m_0m_B, \tag{12}$$

where $\Delta=m_c/m_s$. According to the theory of the "two-band" model,[23] the spin splitting of the energy levels for electrons in bismuth should be equal to the orbital splitting. The predicted condition $\Delta=1$ implies the characteristic degeneracy of energy levels

$$E_{n,s=+1/2}(k_B)=E_{n+1,s=-1/2}(k_B). \tag{13}$$

Experiments on the spin splitting for electrons[5,6] show rather small deviations from the predictions of the two-band model for directions of light cyclotron mass; larger deviations occur in the directions of heavy cyclotron masses, where the validity of the two-band model breaks down. The spin splitting for holes in bismuth[24]

[23] M. H. Cohen and E. I. Blount, Phil. Mag. **5**, 115 (1960).
[24] G. E. Smith, G. A. Baraff, and J. M. Rowell, Phys. Rev. **135**, A1118 (1964).

will be discussed below in connection with the experiments.

The ultrasonic-amplitude-attenuation coefficient $\alpha(B)$ for one ellipsoidal-parabolic energy band is given by the following expression,[4,5,9,10,15,25] which is valid in the "intermediate" region of quantum oscillations, $\omega\tau<1$, $ql\gg1$ (where τ is the relaxation time and l is the mean free path of carriers):

$$\frac{\alpha(B)}{B}=\frac{em_0}{32\pi\hbar^2\rho}\frac{\omega}{kT}\left[(\hat{e}\cdot\mathbf{C}\cdot\hat{q})^2\frac{m_B}{v_s^2\cos\varphi}\right]\times\sum_{n,s}I_n(\gamma)\int_{-\infty}^{+\infty}dy\,\frac{B'/\pi}{1+B'^2y^2}\cosh^{-2}[\tfrac{1}{2}(y^2-A_{n,s})],\quad(14)$$

where ρ is the density, k is Boltzmann's constant, $\varphi=\sphericalangle(\mathbf{q},\mathbf{B})$, $I_n(\gamma)=e^{-\gamma}[L_n^{(0)}(\gamma)]^2$, $\gamma=(\hbar m_c/2eB)(\mathbf{q}\cdot\boldsymbol{\alpha}\cdot\mathbf{q}-q_B^2/m_B)$, and $q_B=\mathbf{q}\cdot\hat{B}$. $L_n^{(0)}(\gamma)$ is the associated Laguerre polynomial.

$$B'=q_Bl_B(kT/E_F)^{1/2}=ql_B\cos\varphi\,(kT/E_F)^{1/2},\qquad A_{n,s}=[E_F-(n+\tfrac{1}{2}+s\Delta)\hbar\omega_c]/kT,\quad(15)$$

and $l_B=v_B\tau=\tau(2E_F/m_B)^{1/2}$ is the mean free path in the direction of the magnetic field, assuming isotropic relaxation time. E_F is the Fermi energy. In the region of giant quantum oscillations, i.e., for high magnetic fields and small quantum numbers n, the quantity $I_n(\gamma)$ is essentially unity.

The function $f(y,B')=B'/\pi(1+B'^2y^2)$ under the integral in Eq. (14) describes the influence of impurity scattering, which was introduced first in an intuitive way by Gurevich *et al.*[9] and later was justified more rigorously.[5,10,15] When $q_Bl_B\to\infty$, the influence of collisions can be neglected; the function $f(y,B')$ behaves like a δ function, and the quantity $\cosh^{-2}\frac{1}{2}A_{n,s}$ describes the line shape of the oscillations. Whenever a Landau level crosses the Fermi energy, $\cosh^{-2}\frac{1}{2}A_{n,s}=1$, and a sharp peak $\alpha_p(B)$ occurs in the ultrasonic attenuation, the height of which can be calculated from Eq. (14), assuming that $\Delta=1$:

$$\alpha_p(B)/B=(\hat{e}\cdot\mathbf{C}\cdot\hat{q})^2(m_B/v_s^2\cos\varphi)\times F(\omega,T)K^{-1}(q_Bl_B),\quad(16)$$

where

$$F(\omega,T)=(em_0/16\pi\hbar^2\rho)\omega/kT.\quad(17)$$

$K=K(q_Bl_B)$ is a correction factor that describes the reduction of the peak absorption due to the influence of collisions, where $K\to1$ for $q_Bl_B\to\infty$ and K increases for decreasing q_Bl_B. According to Eq. (16), the largest attenuation $\alpha_p(B)$ occurs when the magnetic field is applied in the direction of the long axis of the $\boldsymbol{\alpha}$ ellipsoid, where m_B is a maximum. Equation (15) shows that in this case l_B is a minimum (assuming isotropic τ), resulting in the largest amplitude reduction due to collisions. On the other hand, for small m_B the attenuation $\alpha_p(B)$ is small, and the amplitude-reduction factor $K(q_Bl_B)$ is close to unity. The influence of $K(q_Bl_B)$ will be discussed later in more detail in connection with the experiments.

In order to evaluate the deformation-potential components from magnetoacoustic measurements, the anisotropy of $\alpha_p(B)/B$ for different energy bands was measured at constant frequency and temperature, using ultrasonic modes with different $\hat{q}$ and $\hat{e}$ vectors. Defining a reduced attenuation

$$\frac{\alpha_p'(B)}{B}=K\frac{\alpha_p(B)}{B}\frac{\tilde{v}_s^2\cos\varphi}{m_B},\quad(18)$$

with $\tilde{v}_s=v_s\times10^{-5}$ sec/cm, ratios of deformation potentials may be calculated from Eqs. (16) and (18):

$$\pm\left(\frac{[\alpha_p'(B)/B]_r}{[\alpha_p'(B)/B]_s}\right)^{1/2}=\frac{(\hat{e}\cdot\mathbf{C}\cdot\hat{q})_r}{(\hat{e}\cdot\mathbf{C}\cdot\hat{q})_s},\quad(19)$$

where the indices r and s describe different combinations of the band index l and the ultrasonic mode. Absolute values of deformation potentials may be determined from Eq. (16). The sign of the deformation potential cannot be obtained from ultrasonic measurements, since the square of $\hat{q}\cdot\mathbf{C}\cdot\hat{e}$ appears in Eq. (16). The sign is known, however, from piezogalvanomagnetic measurements.[16,17]

III. EXPERIMENTS

A. Experimental Procedure

The ultrasonic experiments were performed at a frequency of 60 MHz and a temperature $T=1.6$°K, using standard pulse-echo techniques. Longitudinal and transverse ultrasonic modes were excited by X- and Y-cut quartz transducers, respectively. The change of ultrasonic attenuation as a function of magnetic field strength up to 16 kG was recorded, using a sampling technique.[3] The direction of magnetic field could be rotated in two orthogonal planes containing the direction of sound propagation $\hat{q}$. The samples were cut from Czochralski-grown single crystals of bismuth[26] (purity 99.9999%) using a spark cutter. The surfaces were polished plane and parallel to within a few seconds of arc. The samples were approximately cube-shaped with edge lengths around 7 mm. The crystallographic orientation was determined using the light-figure method.[27] The sample could be positioned very accurately within the cryostat, using the pronounced "tilt" effect,[1,5] which occurs for magnetic-field directions $\mathbf{B}\perp\mathbf{q}$.

[25] K. H. Sarges (unpublished).

[26] The crystals were kindly supplied by J. M. Noothoven van Goor of Philips Research Laboratories, Eindhoven, The Netherlands.

[27] D. T. J. Hurle and S. Weintroub, Brit. J. Appl. Phys. **10**, 336 (1959).

B. Experimental Results

According to Eq. (16), the peak attenuation $\alpha_p(B)/B$ should be independent of magnetic field strength and should be a function of the direction of $\hat{B}$ only. The attenuation values $\alpha_p(B)/B$ determined experimentally from absorption peaks with different quantum numbers n usually showed a flat maximum as a function of magnetic field strength which occurred for fields intermediate between 4 and 16 kG. This effect was also noted in previous investigations.[5,16] The decrease of $\alpha_p(B)/B$ at higher magnetic fields can be explained by the fact that the spin-splitting degeneracy of energy levels, predicted in Eq. (13), is not exactly satisfied experimentally. For this reason the absorption peaks with small n are split, and the maximum absorption reaches smaller values as compared with the case of complete overlap. For attenuation maxima with larger quantum numbers n (smaller magnetic fields), the overlap between the energy levels within a single absorption peak becomes more complete and the value of $\alpha_p(B)/B$ increases with decreasing B up to a flat maximum. A decrease of $\alpha_p(B)/B$ at very small magnetic fields is to be expected on theoretical grounds [see Eqs. (14) and (15)] in the range of geometrical resonances for B below 1 kG. The decrease of peak attenuation, observed experimentally, occurs already at higher magnetic fields (2–3 kG). In the experimental results reported below, the values of maximum $\alpha_p(B)/B$ are plotted as a function of magnetic field direction, given by the angle φ in Eq. (14). In some cases additional points for absorption peaks close to the maximum of $\alpha_p(B)/B$ are shown for comparison, e.g., in Fig. 3. The theoretical curves for the anisotropy of $\alpha_p(B)/B$ in Figs. 1–6 and 9–11 were calculated from the functions $m_B/\cos\varphi$, using the $\boldsymbol{\alpha}$-tensor components due to Mase *et al.*[5] This case corresponds to neglecting impurity scattering [$q_B l_B \to \infty$ in Eq. (16)]. The theoretical curves are plotted as solid lines and are adjusted for best fit with the experimental points in the region of largest $q_B l_B$.

The measured peak attenuation $\alpha_p(B)/B$ for sound propagation along the binary x axis is shown in Figs. 1–3 as a function of the magnetic field direction. Strong overlap between the oscillations with $l=2$ and 3 occurs for magnetic field directions close to the x axis. For the longitudinal wave, $L(x)$ oscillations due to all energy bands ($l=1$–4) are observed (see Fig. 1), which is to be expected according to Table I. The oscillations with $l=1$ in the x-y plane clearly show the effect of amplitude reduction due to impurity scattering [see Eqs. (15) and (16)], which becomes more pronounced as the magnetic field is rotated towards the y axis. The oscillations with $l=4$ in the x-z plane in Fig. 1 are due to holes; the electron oscillations with $l=1$ are too weak to be observable in the x-z plane. Agreement with the theoretical curve for $l=4$ cannot be expected, since the calculations were done under the assumption of constant spin splitting. In reality the spin splitting of the Landau levels for holes increases from a value $\Delta \ll 1$ [Eq. (12)] for $\mathbf{B} \| \hat{z}$ towards $\Delta \approx 2$ as the direction of the magnetic field is rotated away from the trigonal axis.[24] The fast and slow shear waves $S_1(x)$ and $S_2(x)$ with $\hat{q} \| \hat{x}$ couple only with the electron bands $l=2$ and 3 (see Figs. 2 and 3). The

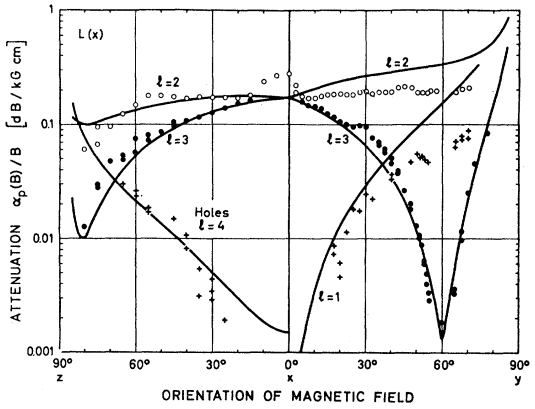

FIG. 1. Peak attenuation $\alpha_p(B)/B$ for longitudinal wave $L(x)$ with $\hat{q} \| \hat{x}$ ($f=60$ MHz, $T=1.6$°K).

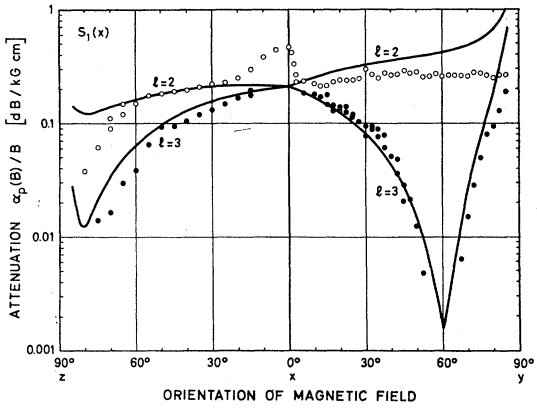

FIG. 2. Peak attenuation $\alpha_p(B)/B$ for fast shear wave $S_1(x)$ with $\hat{q} \| \hat{x}$ ($f=60$ MHz, $T=1.6$°K).

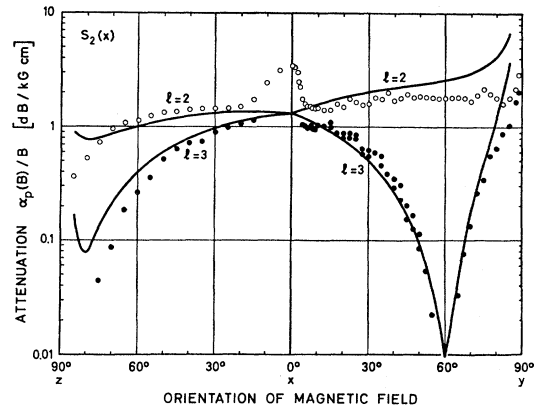

FIG. 3. Peak attenuation $\alpha_p(B)/B$ for slow shear wave $S_2(x)$ with $\hat{q} \| \hat{x}$ ($f=60$ MHz, $T=1.6$°K).

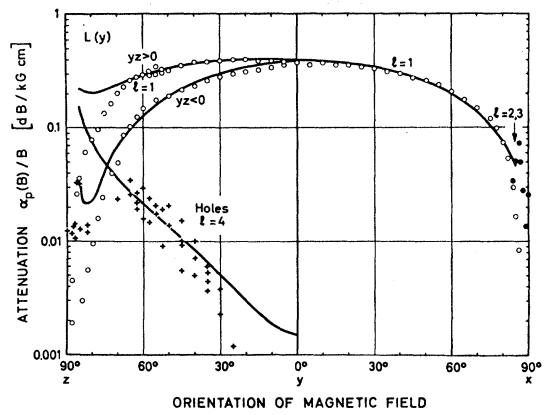

FIG. 4. Peak attenuation $\alpha_p(B)/B$ for quasilongitudinal wave $L(y)$ with $\hat{q}\|\hat{y}$ ($f=60$ MHz, $T=1.6$°K).

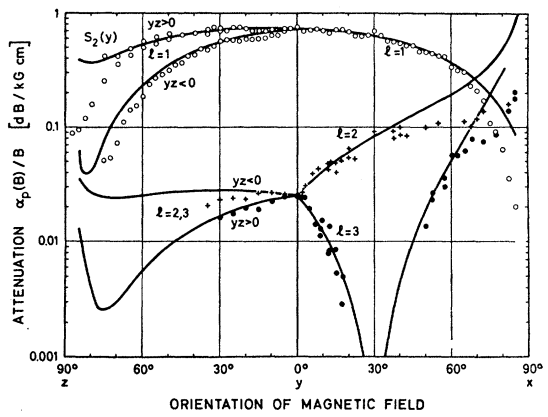

FIG. 5. Peak attenuation $\alpha_p(B)/B$ for quasishear wave $S_2(y)$ with $\hat{q}\|\hat{y}$ ($f=60$ MHz, $T=1.6$°K).

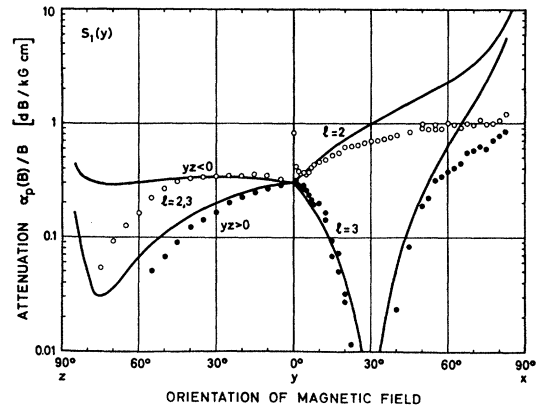

FIG. 6. Peak attenuation $\alpha_p(B)/B$ for pure shear wave $S_1(y)$ with $\hat{q}\|\hat{y}$ ($f=60$ MHz, $T=1.6$°K).

experimental result agrees with the theoretical prediction in Table I. The high value of magnetoacoustic attenuation for the slow shear wave $S_2(x)$ (see Fig. 3) in combination with its low sound velocity (see Table I) makes this wave most suitable for ultrasonic-amplification experiments in the presence of an electric drift field.[28]

The experimental results for wave propagation along the bisectrix y axis are summarized in Figs. 4–6. The quasilongitudinal wave $L(y)$ shows strongest coupling for the $l=1$ electron band (see Fig. 4). Coupling with the electron bands $l=2$ and 3 is extremely weak and could be measured only in the x-y plane for magnetic-field directions near the x axis. The attenuation for $\mathbf{B}\|\hat{y}$ was estimated to be $\alpha_p(B)/B<5\times10^{-4}$ dB/kG cm. The absence of the $l=2$ and 3 oscillations for $L(y)$ was noted by several authors previously[5,6] and was interpreted by Inoue and Tsuji[16] as being due to a special relation between the deformation-potential tensor components (see Table I). For the hole oscillations ($l=4$) in the y-z plane of Fig. 4 the same comment applies as in Fig. 1. The results for the quasishear mode $S_2(y)$ in Fig. 5 show coupling for the electron bands $l=1$, 2, and 3. The overlap between the $l=2$ and 3 peaks in the y-z plane was removed by a slight rotation of the magnetic field perpendicular to the y-z plane. Coupling with the hole band is too small to be observable (see Table I). The experiment confirms (see Fig. 6) that the pure shear mode $S_1(y)$ only couples with the electron bands $l=2$ and 3 (see Table I).

With the magnetic field direction in the x-y plane the experimental curves in Fig. 6 most clearly show the effect of reduction of the attenuation due to impurity scattering, the case of strongest coupling ($\varphi\rightarrow90°$) corresponding to the largest reduction factor $K(q_Bl_B)$. Curves for the dependence $K=K(q_Bl_B)$ were derived from the experiments in the following way: The functions $q_Bl_B=ql_B\cos\varphi$ were calculated from Eq. (15) for the cases $\hat{q}\|\hat{y}$, $L(y)$ ($l=1$), and $S_1(y)$ ($l=2, 3$), and are plotted in Fig. 7 for magnetic field directions in the x-y plane. The calculations were carried out with the mass parameters of Mase *et al.*,[5] $E_{F,e}=17.7$ meV, using the assumption of an isotropic relaxation time for electrons $\tau=1.9\times10^{-10}$ sec, which is approximately satisfied.[29] The correction factor K can be derived from Fig. 6 by comparing the experimental and theoretical curves. By combining K and q_Bl_B values with the same φ in Figs. 6 and 7, the curve $K=K(q_Bl_B)$ can be drawn in Fig. 8, which also contains measured correction factors for ultrasonic modes propagating along the trigonal axis and along the bisector direction between the y and z axes. An average curve $K=K(q_Bl_B)$ is also plotted in Fig. 8. The fit between theory and experiment for the $l=1$ oscillation in the quasilongitudinal wave $L(y)$ with magnetic field directions in the x-y plane is very good for φ up to 80° (see Fig. 4). For this case the value $q_Bl_B=1.55$ is nearly independent of field orientation (see Fig. 7), resulting in a large but constant reduction factor $K=2.18$ according to the averaged curve in Fig. 8. Table II summarizes the following

[28] K. Walther, Solid State Commun. 4, 341 (1966).
[29] R. N. Zitter, Phys. Rev. **127**, 1471 (1962).

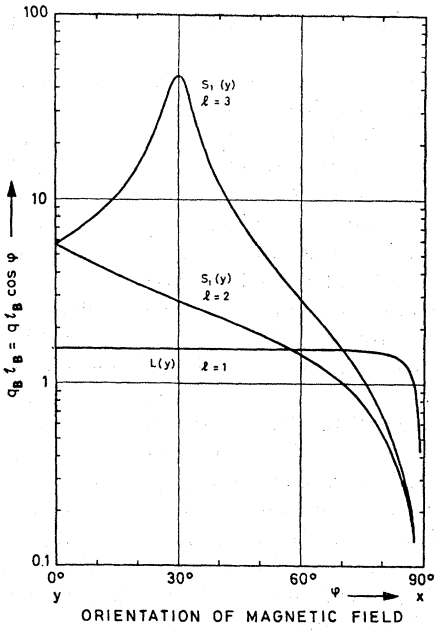

FIG. 7. Calculated values of $q_B l_B$ according to Eq. (15) as a function of magnetic-field orientation in the x-y plane for quasi-longitudinal wave $L(y)$ and pure shear wave $S_1(y)$ with $\hat{q}\|\hat{y}$, using effective-mass parameters of Mase *et al.* (Ref. 5) for electron bands $l=1$, 2, and 3 ($T=1.6$°K), $\tau=1.9\times10^{-10}$ sec).

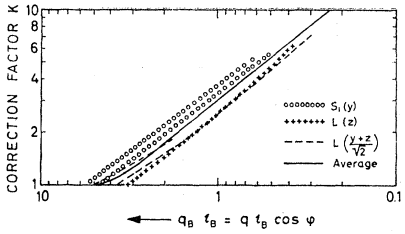

FIG. 8. Correction factor K for attenuation due to impurity scattering, as a function of $q_B l_B$, determined experimentally for various ultrasonic modes. An average curve is also shown.

quantities for various ultrasonic modes and different energy bands in bismuth: (a) measured attenuation $\alpha_p(B)/B$, (b) correction factor K, (c) corrected attenuation $K\alpha_p(B)/B$, and (d) reduced attenuation $\alpha_p'(B)/B$ according to Eq. (18).

Figure 9 shows the measured attenuation for the longitudinal wave $L(z)$ propagating along the trigonal axis. Oscillations due to the electron bands $l=1$, 2, and 3 and the hole band $l=4$ were observed. The reduction effect due to impurity scattering is clearly visible for the electron oscillations as the magnetic field is rotated away from the z direction. This effect was noted previously by Inoue and Tsuji.[16] However, these authors did not give any interpretation. Results for the degenerate shear wave $S(z)$ propagating along the z direction are not given, because the measurements were not very well reproducible. Evidently, interference effects were caused by two slightly different sound velocities of the degenerate shear modes, possibly due to a slight deviation of the propagation direction from the z axis.

The measured attentuation for the quasilongitudinal wave $L(y+z)/\sqrt{2}$ and the quasishear wave $S_2(y+z)/\sqrt{2}$ propagating along the bisector direction between the y and z axes, $\hat{q}\|(\hat{y}+\hat{z})/\sqrt{2}$, is shown in Figs. 10 and 11, respectively. In Fig. 10, absorption peaks due to the electron bands $l=1$, 2, and 3 can be seen. The overlap between the $l=2$ and 3 peaks was removed by a slight rotation of the magnetic field perpendicular to the y-z plane, as in Fig. 5. The effect of impurity scattering on reducing the peak attenuation is clearly visible in Fig. 10. For magnetic field directions close to the z axis ($\varphi=-45°$ in Fig. 10), the attenuation due to the electron band $l=1$ becomes very small. An exact

TABLE II. Reduced attenuation and deformation potentials for various ultrasonic modes in bismuth.

Wave-vector direction $\hat{q}$	Case No.	Mode, band index	$\varphi=\sphericalangle(\hat{q},\mathbf{B})$	Attenuation α_p/B (dB/kG cm)	Correction factor K	Corrected attenuation $K\alpha_p/B$ (dB/kG cm)	Reduced attenuation $\frac{\alpha_p'}{B}=\frac{K\alpha_p}{B}\frac{\tilde{v}_s^2\cos\varphi}{m_B}$	Deformation potential $[(1/a_2)\sum_{i,k}C_{ik}e_i q_k]^2$
$\hat{x}$	1	$L(1)$	60°	0.066	3.2	0.211	0.467	0.1369
	2	$L(2)$	0°	0.17	1.9	0.323	1.619	0.4323
	3	$S_1(2)$	0°	0.21	1.3	0.273	0.536	0.1624
	4	$S_2(2)$	0°	1.30	1.0	1.30	0.755	0.2365
$\hat{y}$	5	$L(1)$	0°	0.40	2.18	0.872	3.484	0.9127
	6	$L(2)$	0°	$<5\times10^{-4}$			$<10^{-2}$	10^{-6}
	7	$S_1(2)$	0°	0.30	1.0	0.30	1.423	0.3519
	8	$S_2(1)$	0°	0.72	1.08	0.778	0.494	0.1464
	9	$S_2(2)$	0°	0.025	1.0	0.025	0.0626	0.01627
$\hat{z}$	10	$L(1)$	0°	0.0022	1.0	0.0022	0.243	0.0841
	11	$L(4)$	0°	0.019		0.019	0.1427	···
$\frac{\hat{y}+\hat{z}}{\sqrt{2}}$	12	$L(1)$	0°	0.25	1.3	0.325	1.309	0.4408
	13	$L(2)$	0°	0.0063	1.0	0.0063	0.203	0.07217
	14	$S_2(1)$	0°			0.75	0.958	0.2401
	15	$S_2(4)$	0°	0.080		0.080	0.1373	···

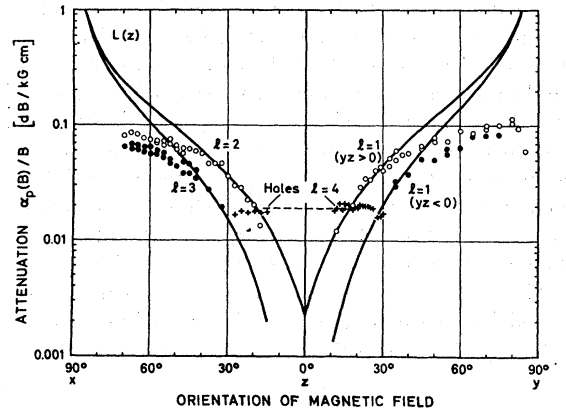

FIG. 9. Peak attenuation $\alpha_p(B)/B$ for longitudinal wave $L(z)$ with $\hat{q}\|\hat{z}$ ($f=60$ MHz, $T=1.6$°K).

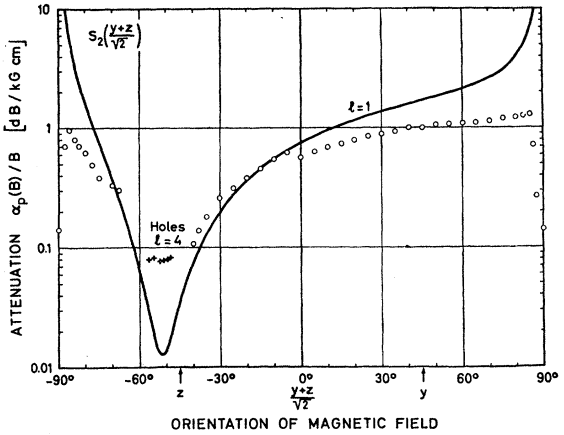

FIG. 11. Peak attenuation $\alpha_p(B)/B$ for quasishear wave $S_2(y+z)/\sqrt{2}$ with $\hat{q}\|(\hat{y}+\hat{z})/\sqrt{2}$ ($f=60$ MHz, $T=1.6$°K).

analysis of the measured periods $\Delta(1/B)$ of the weakly coupling oscillations with $\alpha_p(B)/B\approx 0.004$ dB/kG cm around $\varphi=-50°$ shows that these oscillations are due to the electron bands $l=2$ and 3. No oscillations due to the hole band ($l=4$) were found in the quasilongitudinal wave $L(y+z)/\sqrt{2}$. On the other hand, very strong hole oscillations [identified by their periods $\Delta(1/B)$] are present with the quasishear wave $S_2(y+z)/\sqrt{2}$ for a field orientation close to the z axis ($\varphi=-45°$ in Fig. 11). Coupling with the hole band for $\hat{q}\|(\hat{y}+\hat{z})/\sqrt{2}$ thus shows the opposite behavior as in the cases $\hat{q}\|\hat{x}$, $\hat{y}$, or $\hat{z}$, where strongest coupling is observed for the longitudinal modes. This feature is caused by the structure of the deformation-potential tensor for holes, which will be discussed in Sec. IV.

IV. DETERMINATION OF DEFORMATION-POTENTIAL TENSORS FOR ELECTRONS AND HOLES IN BISMUTH

Linear relations between the tensor components a_1, a_2, and a_4 of the deformation potential for electrons can be obtained from Eq. (19) and Table I using the reduced attentuation $\alpha_p'(B)/B$ for wave propagation along the x and y axes (cases 1–9 in Table II). The linear functions resulting from Eq. (19) and Table I for various combinations r and s are plotted as straight lines in a coordinate system with the axes a_1/a_2 and a_4/a_2 (see Fig. 12). The combination of indices r/s as a parameter at each line in Fig. 12 refers to the case numbers in Table II. Within experimental scatter the straight lines in Fig. 12 define a crossing region centered around

$$a_1/a_2=-0.37, \quad a_4/a_2=+0.25. \tag{20}$$

Equation (19) contains two solutions for each combination r/s because of the sign ambiguity of the square root. The physically significant solutions define a common crossing region with a high statistical weight. They can thus be distinguished unambiguously from the solu-

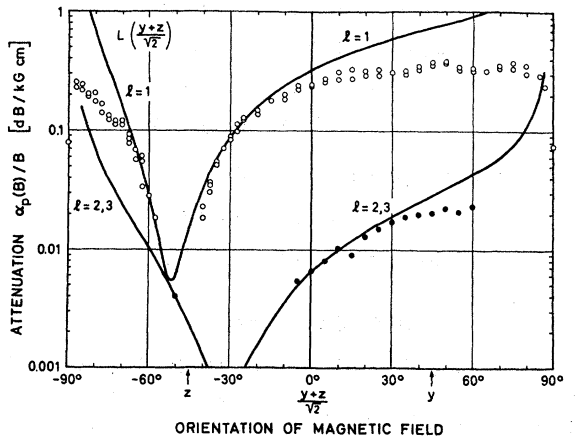

FIG. 10. Peak attenuation $\alpha_p(B)/B$ for quasilongitudinal wave $L(y+z)/\sqrt{2}$ with $\hat{q}\|(\hat{y}+\hat{z})/\sqrt{2}$ ($f=60$ MHz, $T=1.6$°K).

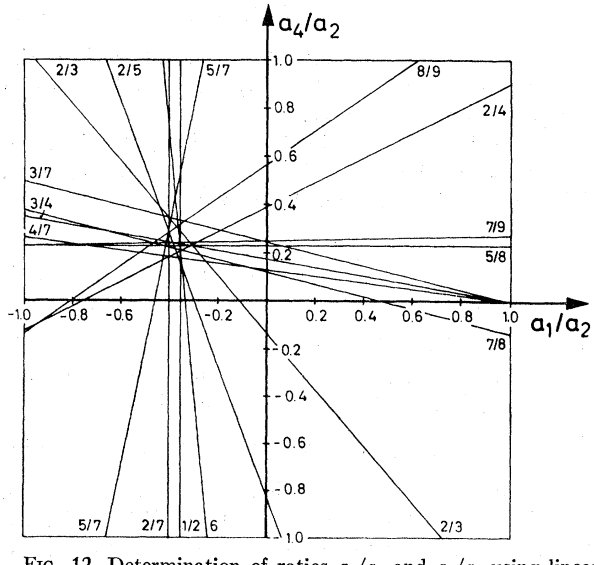

FIG. 12. Determination of ratios a_1/a_2 and a_4/a_2 using linear relations between deformation-potential components according to Eq. (19) and Table I. The indices r/s on each line refer to a combination of case numbers in Table II.

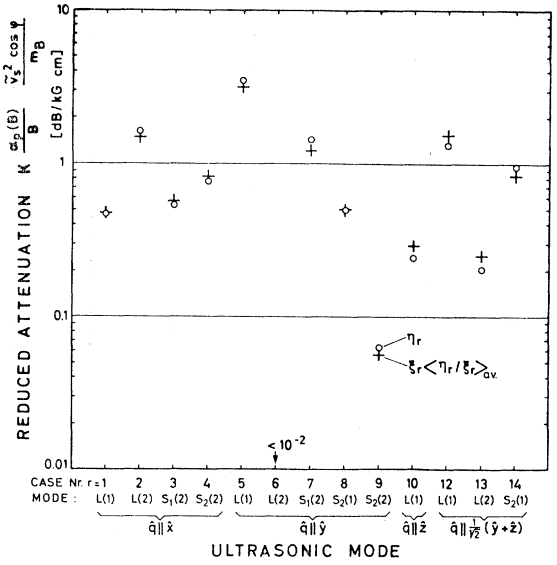

FIG. 13. Anisotropy of measured attentuation $\eta_r=[\alpha_p'(B)/B]_r$ and adjusted values of $\xi_r\langle\eta_r/\xi_r\rangle_{av}$ [ξ_r being given by Eq. (22)], calculated from deformation-potential components for various ultrasonic modes in bismuth.

tions resulting from the mathematical-sign ambiguity in Eq. (19), which are distributed more or less randomly in the (a_1/a_2)-(a_4/a_2) plane without a common crossing region.

The ratio a_3/a_2 can be determined from Eq. (19) and Table I using the values of a_1/a_2 and a_4/a_2 from Eq. (20) and considering cases 10 and 12–14 from Table II with wave propagation along the directions $\hat{z}$ and $(\hat{y}+\hat{z})/\sqrt{2}$. The equations resulting from the six combinations among cases 10 and 12–14 have a common solution with an average value:

$$a_3/a_2=-0.29\pm0.02. \tag{21}$$

The physically insignificant solutions resulting from the sign ambiguity in Eq. (19) scatter randomly and can be rejected unambiguously.

The absolute value of the deformation-potential component a_2 can be determined in the following way: Using Eqs. (20) and (21), the quantities

$$\xi_r=\left(\frac{1}{a_2}\sum_{i,k}C_{ik}e_iq_k\right)_r^2 \tag{22}$$

are calculated for the cases r referring to electrons in Table II. Defining $\eta_r=(\alpha_p'/B)_r$, the average of the ratios η_r/ξ_r from Table II was evaluated as

$$\langle\eta_r/\xi_r\rangle_{av}=3.45\pm0.49\ \text{dB/kG cm}. \tag{23}$$

The value of a_2 can be calculated from Eqs. (14), (16)–(18), and (23), assuming that Eq. (13) holds, i.e., $\Delta=1$. With the parameters $f=60$ MHz, $T=1.6$°K, and $\rho=9.86$ gcm^{-3}, the result is

$$a_2=\pm(5.9\pm0.8)\ \text{eV}. \tag{24}$$

The sign of a_2 cannot be determined from magnetoacoustic measurements. Figure 13 summarizes the experimental values of the reduced attenuation $\alpha_p'(B)/B$ for 13 different cases of electron oscillations (see Table II). The adjusted values of $\xi_r\langle\eta_r/\xi_r\rangle_{av}$ describing the best fit to the anisotropy of the attenuation were calculated with the measured deformation-potential components [Eqs. (20)–(24)] and are shown for comparison as crosses in Fig. 13. The accuracy of the fit is ±14%, the largest single deviation (23%) occurs for case 13.

The deformation potential for holes can be determined from cases 11 and 15 in Table II in combination with Eq. (19) and Table I, resulting in

$$b_2/b_1=-1.03. \tag{25}$$

The other solution of Eq. (19) can be rejected on physical grounds, because the holes do not couple with the quasilongitudinal wave $L(y+z)/\sqrt{2}$ (see Fig. 10). This implies that $b_2/b_1\approx-1$ according to Table I. The absolute value of b_2 can be determined in a similar way as a_2, using $\Delta=0$ in Eqs. (14) and (15):

$$b_2=\pm1.2\ \text{eV}. \tag{26}$$

V. SUMMARY

The tensor components of the deformation potential for electrons and holes in bismuth were evaluated from the anisotropy of quantum oscillations in the magnetoacoustic attenuation measured at a frequency $f=60$ MHz and a temperature $T=1.6$°K. The sign of the deformation potential cannot be determined by this method. However, this information is known from piezogalvanomagnetic measurements,[16,17] and these results are given in parentheses below. The magnetoacoustic investigations allow a very direct determination of deformation potentials. The present results confirm some of the piezogalvanomagnetic measurements and, in addition, yield the shear components.

Deformation potential for electrons:

$$a_1/a_2=-0.37, \quad (-0.40)$$
$$a_3/a_2=-0.29, \quad (-0.31)$$
$$a_4/a_2=+0.25, \quad \cdots$$
$$a_2=\pm5.9\ \text{eV} \quad (-5.3\ \text{eV}).$$

Deformation potential for holes:

$$b_2/b_1=-1.03, \quad (-1.04)$$
$$b_2=\pm1.2\ \text{eV} \quad (-1.1\ \text{eV}).$$

ACKNOWLEDGMENTS

Stimulating discussions with D. Polder, W. Schilz, K. H. Sarges, and W. J. A. Goossens are acknowledged. The author is indebted to R. Schulz for carrying out most of the measurements and to D. Restorff for technical assistance.